

THE OFFICIAL MAGAZINE OF THE OCEANOGRAPHY SOCIETY

# Oceanography

#### CITATION

Gade, M., V. Byfield, S. Ermakov, O. Lavrova, and L. Mitnik. 2013. Slicks as indicators for marine processes. *Oceanography* 26(2):138–149, <http://dx.doi.org/10.5670/oceanog.2013.39>.

#### DOI

<http://dx.doi.org/10.5670/oceanog.2013.39>

#### COPYRIGHT

This article has been published in *Oceanography*, Volume 26, Number 2, a quarterly journal of The Oceanography Society. Copyright 2013 by The Oceanography Society. All rights reserved.

#### USAGE

Permission is granted to copy this article for use in teaching and research. Republication, systematic reproduction, or collective redistribution of any portion of this article by photocopy machine, reposting, or other means is permitted only with the approval of The Oceanography Society. Send all correspondence to: [info@tos.org](mailto:info@tos.org) or The Oceanography Society, PO Box 1931, Rockville, MD 20849-1931, USA.

# Slicks as Indicators for Marine Processes

BY MARTIN GADE,  
VALBORG BYFIELD,  
STANISLAV ERMAKOV,  
OLGA LAVROVA,  
AND LEONID MITNIK

**ABSTRACT.** Monomolecular surface films (“sea slicks”) are well known to dampen small-scale waves at the water surface, thereby influencing transport processes at the air-sea interface. Because of their strong wave-damping capacity, they can often be observed, not just on synthetic aperture radar imagery, but also on imagery acquired in the visible and infrared spectral ranges. Because sea slicks tend to accumulate at the water surface along lines of, for example, current shear in fronts and eddies, they can be used as proxies for observing such marine processes from space. We demonstrate how well sea slicks are suited to indicate marine processes in the coastal zone. A slick’s damping capability depends on the surfactant concentration on the sea surface and, thus, on the compression status of the slick-forming material. Furthermore, we show that slick signatures can be used to derive surface current vectors at higher spatial resolution than that of numerical models.

## INTRODUCTION

Remote sensing of the ocean by airborne and spaceborne sensors has become important for a variety of scientific, technical, and routine monitoring applications. Various satellites equipped with active and passive sensors working at microwave, infrared, and optical frequencies have been launched in recent years, providing numerous images of most parts of the world ocean. Among the several different sensors, synthetic aperture radar (SAR) is probably the most sophisticated because of its high ground resolution (with pixel sizes of 1 m and below) and all-weather capabilities.

After several decades of basic research and the development of advanced instruments, data processing techniques, and theoretical models, radar technology has reached an operational stage. Radar images from a variety of sensors are being used as the main source of information for applications such as oceanographic and meteorological research (Jackson and Apel, 2004), climate research, weather forecasting, ship routing and detection (Mallas and Graber, 2013, in this issue), pollution monitoring (Kim et al., 2010; Jones et al., 2011; Nunziata et al., 2013), and tracking bathymetric changes in

coastal waters. Oceanic and atmospheric phenomena, such as fronts, internal waves (Jackson et al., 2013, in this issue), convective cells and rolls (Foster, 2013, in this issue), surface films and slicks (Caruso et al., 2013, in this issue), and bathymetry in coastal waters (Lehner et al., 2013, in this issue) can be visible on radar images. Parameters such as surface wind speed and direction, the surface wave spectrum, and surface current gradients can be directly inferred from the data (Jackson and Apel, 2004). Radar sensors can provide detailed information on small-scale current variability at a scale not accessible by other means, and they work independent of daylight and cloud coverage. Scientists, commercial service providers, and operational end users throughout the world are increasingly interested in the use of remote-sensing techniques. Space agencies will meet the rising demand with planned launches of several sophisticated spaceborne imaging radars and other remote sensors during the coming years, which will provide an unsurpassed variety of data for a better understanding and monitoring of the ocean-atmosphere system.

Considering the merits and shortcomings of sensors that operate at visible

or microwave frequencies, it is highly appropriate to combine these sensors by placing them on the same platforms and operating them simultaneously. Though conceived some time ago, this simple and obvious idea is just now being partially exploited by some groups who are combining SAR with the Advanced Very High Resolution Radiometer (AVHRR) or Satellite Pour l’Observation de la Terre (SPOT) visible channels (Mitnik et al., 2000; Porter et al., 2001; Mitnik and Dubina, 2010). Comprehensive large-scale experiments such as the Coastal Mixing and Optics Experiment (see Porter et al., 2001) and some individual programs are conducting pilot studies using this technique to address phenomena such as algae blooms, oil spills, internal wave packets, and eddies. All of these studies strongly indicate the very promising potential of a synergistic use of SAR and optical sensors.

The experience described above was gained using sensors operating on board unrelated satellites. In contrast, the Envisat payload included the active microwave Advanced SAR (ASAR), the optical MEdium Resolution Imaging Spectrometer (MERIS), and the infrared Advanced Along-Track Scanning Radiometer (AATSR) sensors. It provided a unique opportunity to undertake dedicated research aimed largely at extending the capabilities of satellite remote monitoring in order to study both the coastal zone and the world ocean as a whole. Indeed, well-established correspondence between SAR and optical (in some cases complemented by infrared) images opened up a wide array of opportunities for all-weather monitoring of phenomena that originate on the sea surface or



Figure 1. ERS-2 synthetic aperture radar (SAR) image (70 km × 70 km, acquired on June, 24, 1997, at 22:29 UTC) of Bering Strait. The narrow dark lines in the lower part of the image are due to sea slicks accumulated along shear currents. Image © ESA, 2007

are surface manifestations of in-water processes. The importance of such concerted surveillance (in terms of simultaneously operating sensors) is manifold, and will be illustrated later with some examples.

In times of high biological activity, biogenic films are often present at the surface in marine coastal waters. They may form structures that are driven by local hydrodynamic processes. Because biogenic films influence backscattering of microwaves and reflectance at near-infrared bands, they may be visible on radar and infrared imagery, thus permitting these processes to be monitored

via their surface manifestations. Taking advantage of these properties, the information content inferred from multisensor satellite imagery of coastal zones can be significantly improved by analyzing signatures of marine surface films. Because of its high resolution and the pronounced effect of surface films at microwave frequencies, the analysis of radar imagery was the core of our investigations.

Processes leading to slick-induced signatures in SAR imagery take place on a wide range of length scales, from submillimeter to hundreds of kilometers. Intermolecular interactions cause

the strong wave damping capabilities of monomolecular surface films (“sea slicks”) that lead to strong damping of water surface waves with lengths of centimeters to decimeters (Alpers and Hühnerfuss, 1989). The accumulation of surface-active material (“surfactants”) on the water surface, and the initial spectral density of those water waves, may in turn depend on (sub) mesoscale to large-scale phenomena such as eddies and fronts, which are often encountered in coastal regions. Sea slicks often accumulate along shear currents, for example, in eddies, as demonstrated in Figure 1. In such images as this ERS-2 SAR view of Bering Strait, the complex surface current field may often be delineated in irregular dark signatures, which in turn are caused by accumulated surfactants. This example SAR image demonstrates how marine surface films, whether of biogenic or anthropogenic origin, may enhance the signatures of marine processes in satellite imagery, and may therefore help in understanding the dynamics of the marine coastal environment.

The aim of this paper is to provide a basic understanding of the way in which marine surface films are manifested in SAR images. First, example results from laboratory experiments are used to demonstrate the two-stage damping of surfactants and to show the dependence of the wave-damping capability of surfactants on their concentration at the water surface. Next, results from field experiments are used to demonstrate how the appearance of marine surface films depends on local environmental conditions. Lastly, we demonstrate how slick manifestations in satellite imagery can be used to infer local current fields, and we provide some conclusions from our work.

## BASIC LABORATORY STUDIES

The interpretation of slick signatures in radar images requires an understanding of the generation and damping of the surface waves that are responsible for radar backscattering (Bragg waves). These waves can be freely propagating, or they can be bound to waves of decimeter wavelength, whose spectral density may be influenced by sea slicks (Gade et al., 1998b; Ermakov et al., 2006).

Laboratory measurements were conducted in the University of Hamburg wind-wave tank, which is 26 m long, 1 m wide, and filled with freshwater at a mean depth of 0.5 m. At a wind speed of  $3 \text{ m s}^{-1}$ , small patches of the surface-active substance palmitic acid methyl ester (abbreviated as PME,  $75 \text{ mmol L}^{-1}$  ethanol) were carefully deployed at a fetch of 5.5 m using a pipette. Hühnerfuss et al. (1996) showed that this substance, deployed with the help of a spreading solvent, is well suited for simulating biogenic marine surface films because of its similar spectral wave damping behavior. By varying the duration of their deployment, slicks of different lengths were produced. An overflow baffle and a permanent inflow of freshwater ensured a minimal overflow at the leeward tank end. The aim of these experiments was to demonstrate the effect of slick morphology (i.e., the small-scale arrangement of the slick-forming molecules) on the damping capability of the substance.

A 10 GHz (X-band) scatterometer and a video (CCD) camera were both looking upwind at the same spot on the water surface, at 14.5 m fetch and under an incidence (look) angle of  $38^\circ$ . We produced diffuse light conditions by illuminating the tank roof from

below with two floodlight spots (located beside the tank). Wismann et al. (1998) and Gade et al. (1998b) showed that the radar contrast (i.e., the ratio of the backscattered radar power from outside and inside the slick-covered area) of quasi-biogenic slicks is similar at C-, X-, and Ku-bands at oblique incidence angles, and they found no dependence on the radar polarization. The wave slope in the center of the camera's and scatterometer's footprints was measured by a two-dimensional laser slope gauge. Video images ( $768 \times 494$  pixels) were recorded at a frequency of 2 Hz. By applying a moving Fast Fourier Transform (FFT) algorithm (length 256 and overlap 128) to the initial time series of the scatterometer and laser slope gauge, we obtained time series of the radar backscatter and of the root mean square (rms) slope, respectively, with the same temporal resolution as the video image series (i.e., 2 Hz). All time series were then smoothed by applying a moving, length-3 boxcar filter.

Figure 2 shows results from measurements with PME deployed for 60 seconds. The time series of the downwind and crosswind wave slopes (upper panel, solid and dashed curves, respectively) clearly show the influence of the slick on the wave field: after about 60 seconds with a slick-free water surface (section A), we measured a stepwise decrease in the wave slope (B, length

about 30 seconds). The "trough" of the curve (C) is about 60 seconds long, which corresponds to the deployment duration of PME. After a weak stepwise increase (D), section E is again slick-free. Apparently, a 60-second deployment of PME changed the wave field for about 115 seconds (from 60 to 175 seconds elapsed time); however, we note that the length of the trough corresponds very well to the deployment time. Following Wu (1975) and our own measurements, it takes about 92 seconds for the upper water layer to move from the point of slick deployment to the measurement point because of the wind-induced surface drift. This is about the (elapsed) time when the second step (between sections B and C) occurred, implying that the "main" slick was drifting by between 95 seconds and 155 seconds elapsed time, causing maximum wave damping. The slick's front, which arrived at the measurement point after about 60 seconds, was generated by its forward spreading edge and caused the first stepwise decrease in wave slope (between sections A and B). This finding also explains the second step at the back (windward) edge of the slick (section D), which is shorter, because the slick was drifting against the wind.

It is of particular interest that neither of the remote sensors (the scatterometer and the video camera) sensed a stepwise arrival (and departure) of the slick.

---

**Martin Gade** ([martin.gade@uni-hamburg.de](mailto:martin.gade@uni-hamburg.de)) is a scientist at the Institut für Meereskunde, Universität Hamburg, Hamburg, Germany. **Valborg Byfield** is Research Fellow, National Oceanography Centre, Southampton, UK. **Stanislav Ermakov** is a scientist at the Institute of Applied Physics, Russian Academy of Sciences (RAS), Nizhny Novgorod, Russia. **Olga Lavrova** is Head, Space Research Laboratory, Space Research Institute, RAS, Moscow, Russia. **Leonid Mitnik** is Head, Satellite Oceanography Laboratory, V.I. Il'ichev Pacific Oceanological Institute of RAS, Vladivostok, Russia.

The middle panel of Figure 2 shows the radar Doppler shift and backscatter (upper dashed curve and lower solid curve, respectively). The two steps in the measured Doppler shifts are well correlated with those of the rms wave slope. However, at the same time, we measured a continuous decrease in radar backscatter. The troughs of both curves

are longer than those of the time series for the wave slopes, with an overall length of about 75 seconds. After a steep increase, both curves return to high values. The mean video image intensity (lower panel of Figure 2) increased when the water surface was slick-covered, which agrees with earlier findings (Cox and Munk, 1955). Note that no

stepwise increase (or decrease) was measured, but there was a plateau of about 90 seconds. Moreover, the contrast at the forward (leeward) slick edge seems to be sharper than the contrast at the back (windward) edge.

Similar reductions of the radar Doppler shift were found earlier (Gade et al., 1998a; Ermakov et al., 2006) and were explained by means of the damping of Bragg waves, which are bound to the dominant waves. The remaining free Bragg waves cause a smaller Doppler shift because of their lower phase velocity. Note that we measured a monotonous reduction of the backscattered radar power in section B (Figure 2, top panel), where free Bragg waves are regenerated at the leeward side of the main slick. Thus, the PME slick showed a different damping behavior along its upwind/downwind profile. This is likely to be caused by the fact that the compression status (i.e., the mean area per slick molecule) is different in the main slick and in the areas of slick spreading, which causes a different morphology (Hühnerfuss, 2006) and, in turn, different visco-elastic properties. Our results imply that optical and microwave sensors may provide different results in terms of the spatial coverage of marine surface films, depending on wind speed and the slick's morphology (compression status).

Further investigations of short wind waves and their variability due to long waves were carried out in the oval wind-wave tank of the Institute of Applied Physics, Russian Academy of Sciences (IAP-RAS), Nizhny Novgorod, at low wind conditions and short fetches and in the presence of surfactants at different concentrations. The tank's dimensions are 6 m × 4 m, the total height and

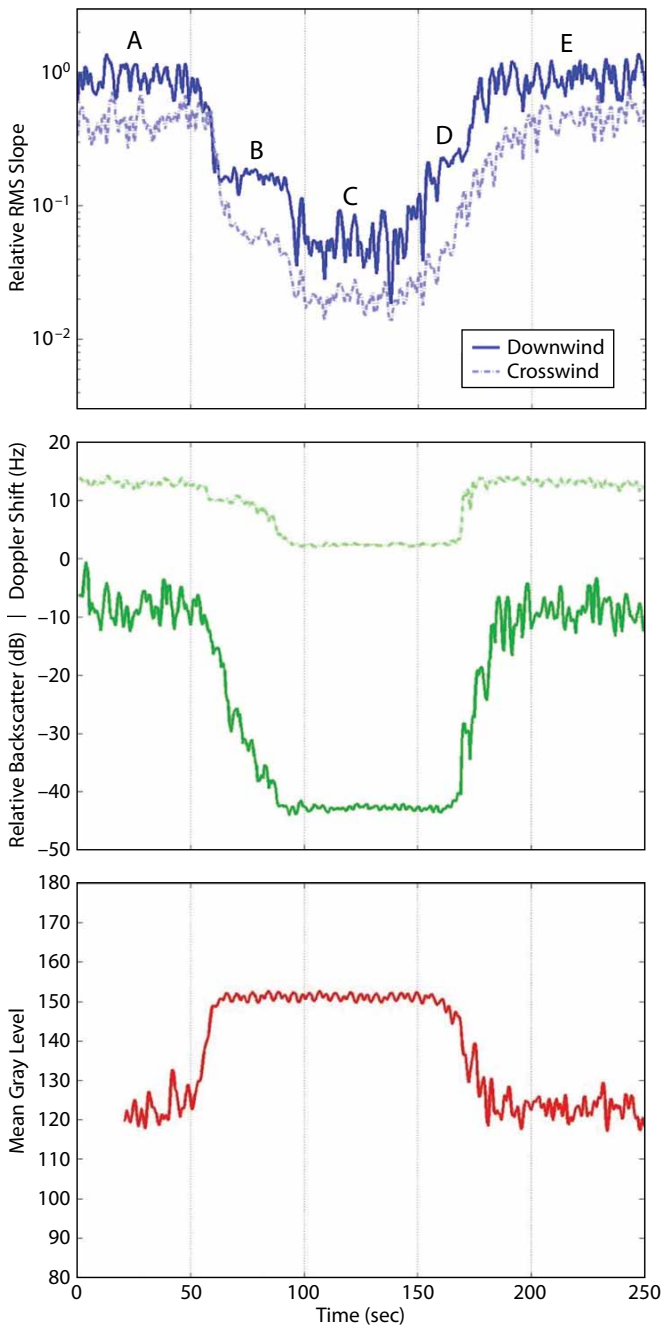


Figure 2. (upper panel) Time series of downwind and crosswind wave slope (dark and light blue curve, respectively). (middle panel) Time series of radar Doppler shifts and radar backscatter (upper and lower curve, respectively). (lower panel) Time series of mean image gray levels. Data were acquired while a small (60 seconds) palmitic acid methyl ester (PME) slick was drifting by. Wind speed was  $3 \text{ m s}^{-1}$ .

width are 0.59 m and 0.3 m, respectively, and the mean water depth is approximately 0.3 m (Ermakov et al., 2006). Wind waves were measured using an optical spectrum analyzer and a coherent Doppler Ka-band radar (35 GHz) operating at an incidence angle of 45°. Surface films in the wind-wave tank were formed by oleic acid. The radar contrast was measured as a function of the surfactant concentration.

Figure 3 shows some typical experimental results. The results were combined with theoretical values obtained assuming purely free or purely bound Bragg waves. In the former case, the radar contrast should be solely associated with the reduction in spectral energy of the Bragg waves. In the latter case, the spectral energy of the generating (decimeter) waves has to be considered. The respective theoretical curves are added in Figure 3. At low wind speeds ( $2 \text{ m s}^{-1}$ ), the measured contrasts indicate that

bound Bragg waves dominate the radar backscattering. We can therefore conclude that the spectral density of the generating (parent) decimeter waves has to be considered in radar backscattering models, particularly at low wind speeds. In this respect, our results may complement recent investigations on these radar scattering mechanisms with and without biogenic slicks using the two-scale Boundary Perturbation Method scattering model (Nunziata et al., 2009), where the surface slick was supposed to modify both the full-range sea surface spectrum and the slope probability density function through Marangoni damping and a reduction of the friction velocity.

### FIELD EXPERIMENTS

An experimental campaign was conducted in August 2004 in the coastal zone of the Black Sea at the South Branch of the Shirshov Institute of Oceanology. The objectives of the

fieldwork were to: (1) develop a better understanding of mechanisms of slick formation and of the relationship between slick geometry and the structure of surface currents, (2) investigate the physical characteristics of marine films, and (3) investigate surfactant spreading regimes.

A new methodology for measuring surface currents in a thin surface layer (about 5 mm) was developed at IAP-RAS using special floats whose trajectories were traced from a small boat using GPS navigation. Simultaneous sampling of the sea surface layer was carried out from a small boat, both within the slicks and in the surrounding non-slick areas. We found that surfactants associated with surface currents accumulate in shear current zones when there is a weak transverse current (Figure 4). This current results in compression of the surfactants and, thus, in stronger wave damping along the shear lines. Figure 4

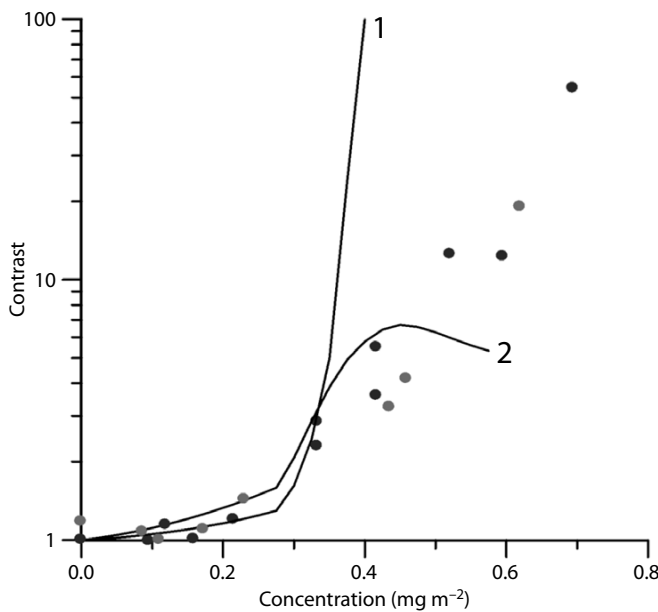


Figure 3. Radar contrast vs. surface concentration of an oleic acid film at  $2 \text{ m s}^{-1}$  wind speed. The dots represent experimental data. Curve 1 denotes theoretical values for freely propagating Bragg waves and curve 2 for bound Bragg waves.

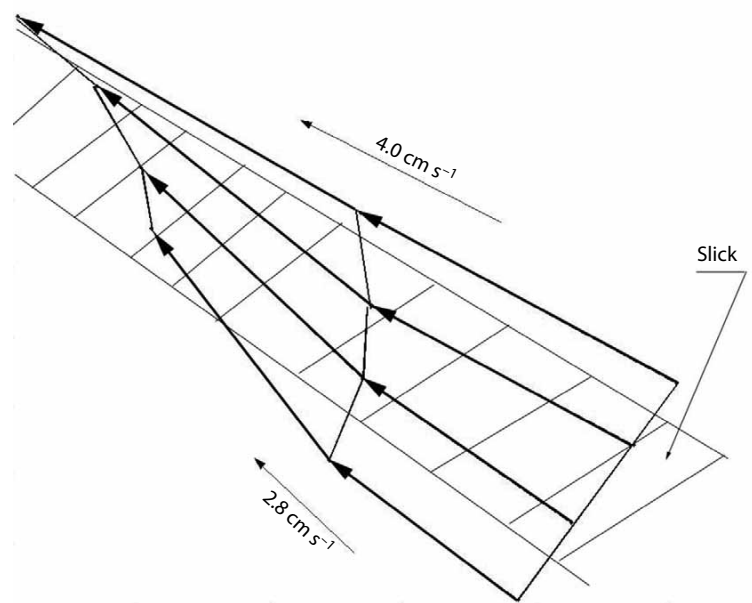


Figure 4. Schematic showing the trajectories of markers, two inside and two outside a natural slick band.

provides an example of float trajectories, two of which were initially placed inside a slick band and another two outside the band. This is why, under favorable environmental conditions, marine surface films may act as tracers for turbulent surface currents such as submesoscale oceanic eddies (Johannessen et al., 1996; Mityagina et al., 2010; Karimova, 2012, Karimova and Gade, in press).

In July, September, and October 2004 and in February 2005, scientists of the V.I. Il'ichev Pacific Oceanological Institute carried out a series of field experiments at their marine station, Cape Shults, located in Vityaz Bay (Peter the Great Bay), Sea of Japan (Figure 5). The main task was to conduct subsatellite optical and hydro-meteorological measurements to improve the interpretation of SAR data and to compare the measured and computed values of the

normalized radar cross section. The field experiments were carried out in different seasons, thus providing a data set well suited for investigating the slick damping processes under different environmental conditions (Mitnik et al., 2006). Optical devices (several video cameras and a polarization spectrophotometer) were deployed to derive the characteristics of gravity and gravity-capillary waves parallel to SAR image acquisitions (results not shown here). The characteristics were estimated from displacements of a system of light floats, as well as from variations of sea surface brightness at three polarizations recorded at frequencies of 6–50 Hz. Narrow bands of artificial oleic acid slicks were created from a yacht prior to ERS-2 and Envisat overpasses (Figure 5). The slick bands were initially about 4–6 m wide and were invisible on the Envisat ASAR images

acquired at the time of the experiment (Figure 6). During the SAR acquisition, moderate northwest winds of 10 kts ( $5 \text{ m s}^{-1}$ ; see the wind arrows in Figure 6) were reported in that area, which caused favorable conditions for SAR imaging of marine surface films. We note that the reference wind speed of  $3 \text{ m s}^{-1}$  used for our laboratory experiments (see Figure 2) roughly corresponds to the same wind speed at a reference height of 10 m. Hydrographic data revealed an oceanic front parallel to the coast at a distance of about 20 km.

### SATELLITE DATA

ERS-2 and Envisat ASAR images were analyzed with respect to manifestations of sea slicks driven by coastal dynamic processes. At wind speeds below  $5\text{--}6 \text{ m s}^{-1}$ , biogenic slicks may indicate various oceanic dynamic phenomena. In this respect, coastal mountains, a complicated coast line, and islands, in combination with (shallow) bottom topography and surface currents, can often be responsible for the generation of eddies, internal waves, and coastal fronts.

Figure 7 shows transects along lines A and B in Figure 6 for horizontal (black) and vertical (grey) polarization. At both polarizations, the strong accumulation of sea slicks (caused by an oceanic front) in transect A results in a radar contrast of more than 10 dB, whereas the surface film (likely a weathered oil spill) in transect B causes a radar contrast of less than 5 dB. Alpers and Hühnerfuss (1988) suggested that surface-active compounds of weathered oil on the sea surface may cause wave-damping behavior similar to that of biogenic surface films (Marangoni damping). However, even if the two surface films observed in



Figure 5. Aerial photograph of Vityaz Bay taken while artificial oleic acid slicks were deployed from a yacht (left). The slicks show up as bright bands behind the yacht and in the foreground.

the Envisat ASAR image had consisted of the same surface-active substance (which is unlikely), their wave damping capability would have been different because the transect A surfactants were compressed along the oceanic front, while those in transect B were spreading freely. The results of our laboratory experiments clearly indicate that this would result in a different damping capability. We note, however, that the difference in radar contrast may be attributed primarily to the surface films being made up of different materials.

Satellite observations of vortical activity in the northeastern part of the Black Sea have been routinely carried out with the help of infrared or optical sensors. The spatial resolution of such images makes it possible to study eddy structures with diameters of more than 30 km. These mostly anticyclonic eddies are referred to as nearshore anticyclonic eddies. Because of their convergence property, they accumulate polluted water and thus contribute to clearing of area waters (Zatsepin et al., 2003).

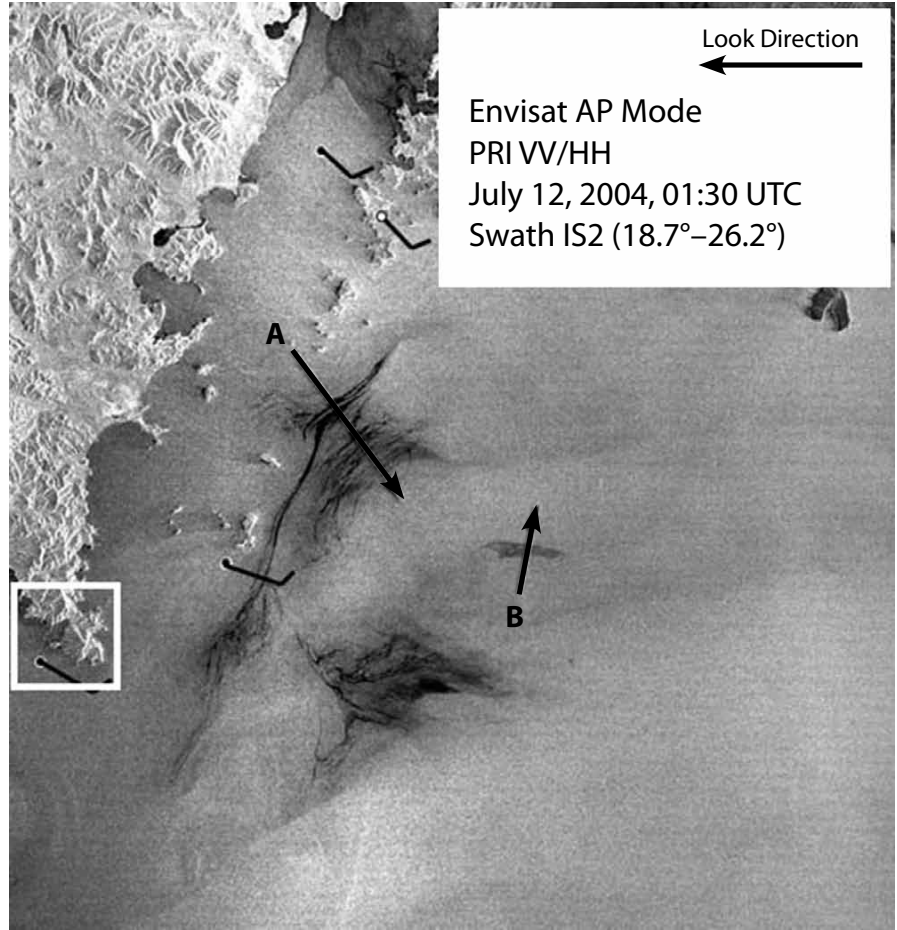


Figure 6. Envisat Advanced SAR image (ASAR; VV polarization, 100 km × 100 km) acquired during the field experiments in Vityaz Bay, Sea of Japan (see the white square on the left). Normalized radar cross section transects were calculated along lines A and B (see Figure 7). The four wind arrows indicate a northwest wind direction at the time of SAR acquisition. Image © ESA, 2004

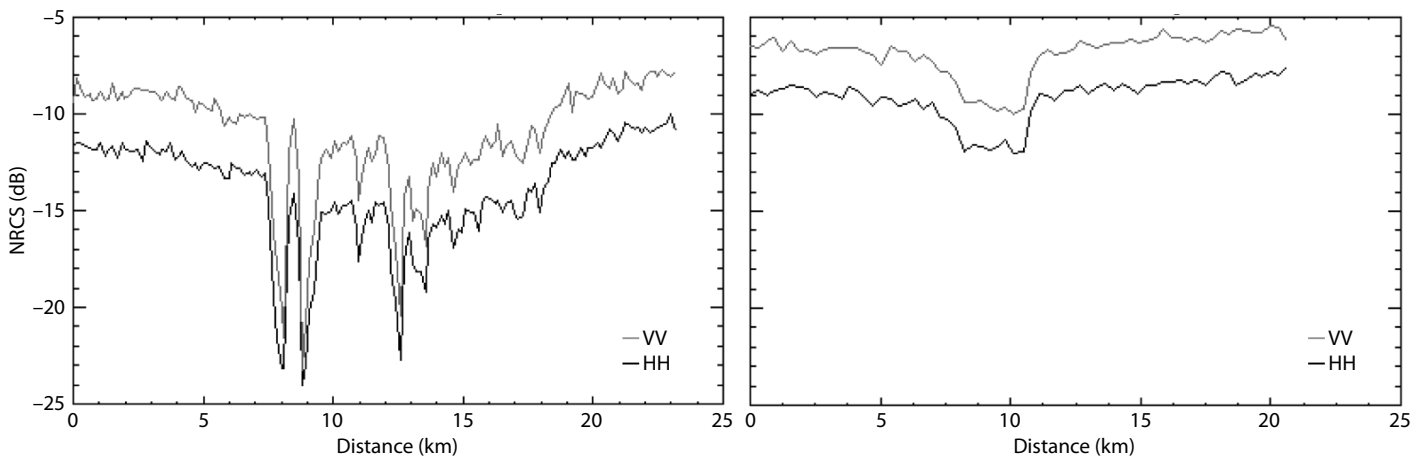


Figure 7. Normalized radar cross section (NCRS) calculated along lines A and B indicated in the Figure 6 SAR image. The upper, gray curves denote vertical (VV) polarization. The lower, black curves denote horizontal (HH) polarization.

The use of SAR data allowed us to discover intense vortex structures of considerably smaller dimensions in this region. Being too small to be detected by the optical or infrared sensors used for our investigations, these small eddies are visualized in SAR images as numerous bands of slicks. Our SAR image analyses revealed that many cyclonic spiral eddies with diameters of a few kilometers to tens of kilometers can be seen in radar images of coastal waters. The cumulative contribution of these small vortices to the transport of pollutants and cleaning of water is comparable to that of large anti-cyclonic eddies (Mityagina et al., 2010). As an example, Figure 8 shows two small cyclonic eddies in a 25 km × 25 km fragment of an Envisat ASAR image acquired on August 15, 2006, over the northeastern Black Sea. The eddies' diameters are less than 4 km, and their lateral structures can be easily seen because of the presence of surface films, which become entrained in convergence zones along the

shear current lines and, because of their strong damping capability, allow visualization of the eddies.

SAR data from all Envisat transits over the northeastern Black Sea were analyzed for the periods from April to November of 2006 and 2007. This allowed us to systematize the data and compile some statistics on small-scale eddies in coastal waters. Every SAR image was visually analyzed to detect structures that could definitively be identified as small-scale spiral eddies. For each eddy, geometrical size, rotational sign, and center coordinates were determined, and all detected eddies were mapped. Figure 9 presents a cumulative chart of small-scale coastal eddies based on analysis of ASAR data. The mapped eddies naturally divide into two distinct groups. Green marks correspond to data obtained in relatively cold periods, between mid-September and mid-May, while magenta marks indicate data from warm summer periods. A dotted curve

traces the conventional core line of the Rim Current—a permanent current system encircling the Black Sea basin cyclonically over the continental slope.

The seasonal variability of small-scale eddies in the coastal waters of the northeastern Black Sea was revealed based on our ASAR image analyses. In the warm season, mostly small-scale (2–6 km in diameter) solitary eddies were observed. Predominantly cyclonic structures, they are located in the immediate vicinity of the coastline and have short lifetimes. In cold seasons, both cyclonic and anti-cyclonic eddies are observed; they are larger, 4 to 25 km, and tend to accumulate in clusters. These clusters are located at the seaward side of the Rim Current about 30 km off the coastline. Figure 10 shows a SAR image of an aggregation of eddies characteristic of cold seasons.

Eddy structures of another type can also be observed in the coastal zone. They are quasi-symmetric, made up of a narrow jet with a pair of vortices of opposite signs at each end. They are referred to as eddy dipoles, or mushroom-like flows. The structures are visible when there is a natural tracer of some kind on the surface or a temperature contrast. In the SAR images, they are visualized as dark filaments due to ripple damping by biogenic surfactant films. Eddy dipoles exhibit no seasonal variability. They usually range in size from tens to hundreds of kilometers. Well-developed eddy dipoles may be distinctly visible in infrared and optical data, but, of course, under cloudless conditions. The use of radar data makes it possible to observe the very first stages of eddy dipole formation (Mityagina et al., 2007). Dynamic vortex structures of this kind regularly observed in this region of

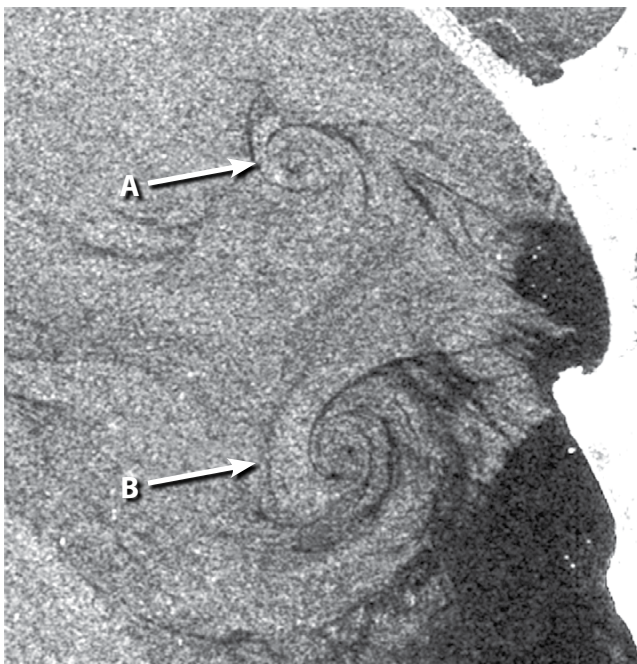


Figure 8. 25 km × 25 km section of an Envisat ASAR image collected August 15, 2006, showing imprints of two cyclonic eddies with mean diameters of 3.75 km (A) and 3 km (B). Their lateral structures can easily be seen because of the presence of surface films. Image © ESA, 2006

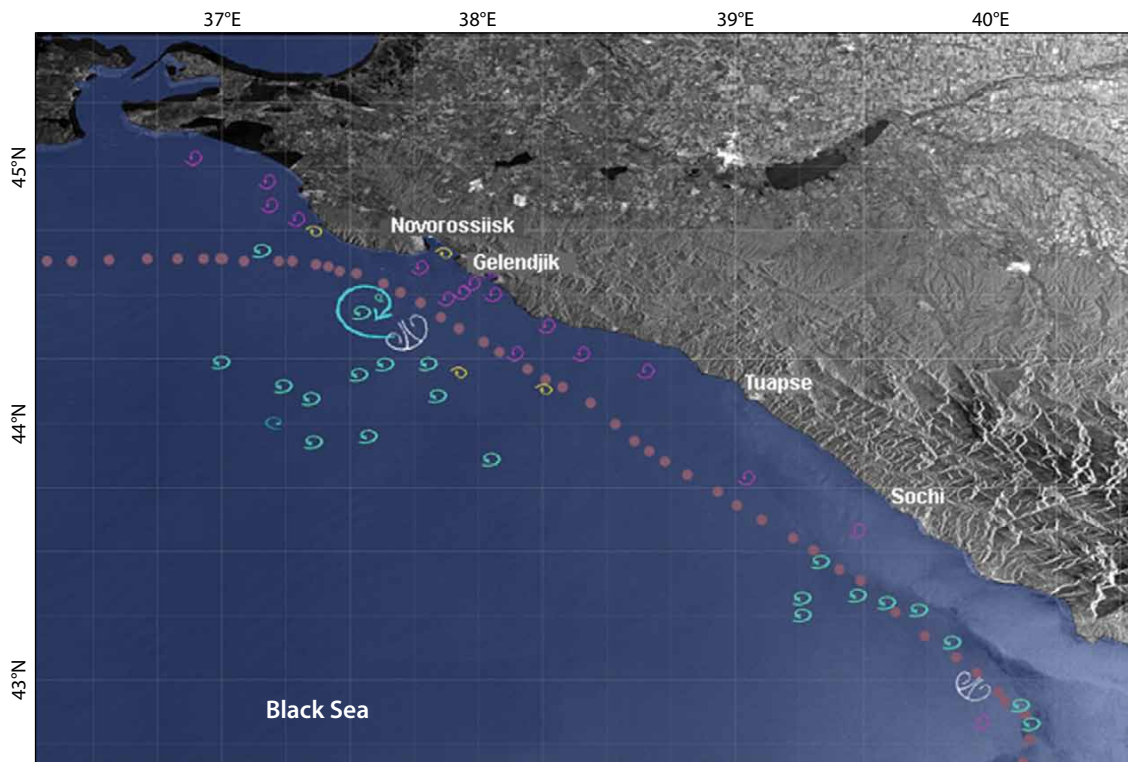


Figure 9. Schematic of small-scale eddies in the coastal waters of the northeastern Black Sea retrieved from Envisat ASAR imagery. Blue-green marks correspond to small-scale eddies observed during relatively cold periods, between mid-September and mid-May. Magenta marks denote the location of small-scale eddies observed on the images during warm summer periods. Dots depict the core line of the Rim Current.

the Black Sea are known to induce not only horizontal but also vertical mixing. They contribute to hydrodynamic instability of the alongshore current and intensify coastal water transport to the open sea.

Two Envisat ASAR images were acquired on June 19, 2006, with a time lag of about 11 hours (Figure 11a,b). The image obtained at 07:52 UTC reveals a nascent eddy dipole (Figure 11a). The dipole seen in the second image (Figure 11b) is somewhat bigger, and its axis is slightly rotated clockwise. Analysis of these two images allows reconstruction of the local velocity field and retrieval of drift parameters of the biogenic films driven by the eddy dipole (Figure 11c). The calculated velocity of its cyclonic fraction is  $0.05\text{--}0.1\text{ m s}^{-1}$  toward the northwest, and the southeast anticyclonic velocity is  $0.2\text{--}0.3\text{ m s}^{-1}$ .

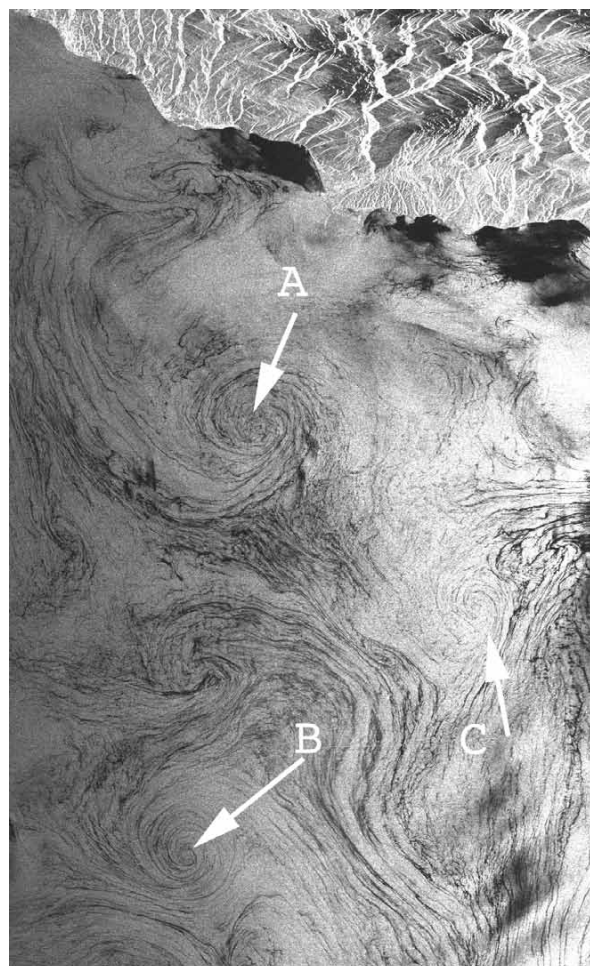


Figure 10. 120 km  $\times$  200 km section of an Envisat ASAR image collected May 10, 2007. Cyclonic eddies with diameters of 22.5 km (A), 25 km (B), and 16 km (C) are clearly visible. Image  $\copyright$  ESA, 2007

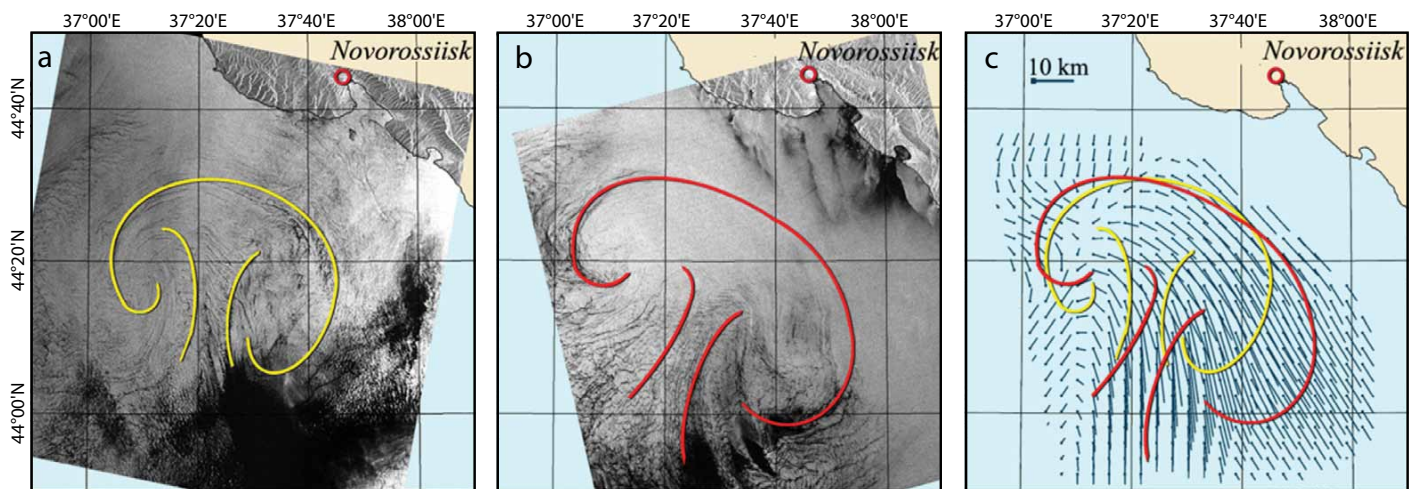


Figure 11. (a) Envisat ASAR image obtained June 19, 2006, at 07:52 GMT showing a nascent dipole eddy. Dimensions are about 66 km x 62 km. © ESA, 2006 (b) Envisat ASAR image of a 92 km x 78 km dipole eddy obtained June 19, 2006, at 19:10 GMT © ESA, 2006 (c) Reconstruction of the local velocity field from analysis of images a and b.

## CONCLUSIONS

Biogenic films can be found virtually everywhere on the vast sea surface, mostly during warm seasons. These films are the result of the life processes of marine organisms and seaweeds, primarily phytoplankton and zooplankton, as well as bacteria. Our experimental results show that biogenic films are very sensitive to surface currents and, as a consequence, indicate the shapes of local circulation patterns. Water dynamics force biogenic films to accumulate along the flow lines of surface currents and in this way emphasize vortex structures, fronts, ship wakes, and other surface ocean features. Because the films influence the backscattering of microwaves, these structures are visible in SAR imagery. This allows monitoring of ocean dynamics processes via their surface manifestations.

We can improve and extend the information that can be inferred from satellite imagery of coastal zones by analyzing signatures of marine surface films (Gade et al., 2005). In particular, due to the presence of surfactant films, SARs are

capable of registering eddy structures. Surfactant films become entrained in eddy motion and, under low to moderate wind conditions, the eddy structures are then apparent in radar images (Lavrova et al., 2008).

During its three-year duration, the international project Slicks as Indicators of Marine Processes (SIMP) provided a wealth of new results on various marine processes whose imprints on satellite imagery are enhanced by marine surface films of biogenic and anthropogenic origin. The investigations performed by the six participating teams comprise laboratory and field experiments as well as comprehensive analyses of satellite data. Our results, some of which are described in this article, provide a basic understanding of the way marine surface films manifest themselves in SAR imagery.

## ACKNOWLEDGMENTS

The work presented here was carried out with the help of several colleagues at the participating institutions. The authors are grateful to Tatiana Bocharova, Anton Churyumov, Denis Darkin,

Vyacheslav Dubina, Susanne Fangohr, Lev Gushchin, Oleg Konstantinov, Philipp Lange, Konstantin Litovchenko, Eugeny Makarov, Marina Mityagina, Irina Sergiewskaya, and Yuri Shchegolkov. The ERS and Envisat satellite data were provided by the European Space Agency (© ESA) through Bear AO 2775, AO3-401, AO3-1291, and AO-ID-391. SIMP, and its follow-on project, Monitoring of Oil Pollution using Earth Observation Data (MOPED), received funding under contracts INTAS 03-51-4987 and INTAS 06-100025-9091, respectively. Further support was granted by the Russian Government through project No. 11.G34.31.0078. We thank two anonymous reviewers for their valuable comments and suggestions.

## REFERENCES

- Alpers, W., and H. Hühnerfuss. 1988. Radar signatures of oil films on the sea surface and the Marangoni effect. *Journal of Geophysical Research* 93(C4):3,642–3,648, <http://dx.doi.org/10.1029/JC093iC04p03642>.
- Alpers, W., and H. Hühnerfuss. 1989. The damping of ocean waves by surface films: A new look at an old problem. *Journal of Geophysical Research* 94(C5):6,251–6,265, <http://dx.doi.org/10.1029/JC094iC05p06251>.

- Caruso, M.J., M. Migliaccio, J.T. Hargrove, O. Garcia-Pineda, and H.C. Graber. 2013. Oil spills and slicks imaged by synthetic aperture radar. *Oceanography* 26(2):112–123, <http://dx.doi.org/10.5670/oceanog.2013.34>.
- Cox, C., and W. Munk. 1955. Some problems in optical oceanography. *Journal of Marine Research* 14:63–78.
- Ermakov, S.A., I.A. Sergiewskaya, E.M. Zuikova, V.Yu. Goldblat, and Yu.B. Shchegolkov. 2006. Wave tank study of phase velocities and damping of gravity-capillary wind waves in the presence of surface films. Pp. 129–143 in *Marine Surface Films*. M. Gade, H. Hühnerfuss, and G. Korenowski, eds, Springer, Heidelberg.
- Foster, R. 2013. Signature of large aspect ratio roll vortices in synthetic aperture radar images of tropical cyclones. *Oceanography* 26(2):58–67, <http://dx.doi.org/10.5670/oceanog.2013.31>.
- Gade, M., W. Alpers, S.A. Ermakov, H. Hühnerfuss, and P.A. Lange. 1998a. Wind-wave tank measurements of bound and freely propagating short gravity-capillary waves. *Journal of Geophysical Research* 103(C10):21,697–21,710, <http://dx.doi.org/10.1029/98JC00778>.
- Gade, M., W. Alpers, H. Hühnerfuss, V. Wismann, and P.A. Lange. 1998. On the reduction of the radar backscatter by oceanic surface films: Scatterometer measurements and their theoretical interpretation. *Remote Sensing of Environment* 66:52–70, [http://dx.doi.org/10.1016/S0034-4257\(98\)00034-0](http://dx.doi.org/10.1016/S0034-4257(98)00034-0).
- Gade, M., S.A. Ermakov, O.Yu. Lavrova, J.C.B. da Silva, and D.K. Woolf. 2005. Using marine surface films as indicators for marine processes in the coastal zone. Pp. 1,405–1,416 in *Proceedings of the 7<sup>th</sup> International Conference on the Mediterranean Coastal Environment (MEDCOAST 2005)*, October 25–29, 2005, Kusadasi, Turkey.
- Hühnerfuss, H. 2006. New chemical insights into the structure and morphology of sea slicks and their geophysical interpretation. Pp. 37–44 in *Marine Surface Films*. M. Gade, H. Hühnerfuss, and G. Korenowski, eds, Springer, Heidelberg.
- Hühnerfuss, H., W. Alpers, H. Dannhauer, M. Gade, P.A. Lange, V. Neumann, and V. Wismann. 1996. Natural and man-made sea slicks in the North Sea investigated by a helicopter-borne 5-frequency radar scatterometer. *International Journal of Remote Sensing* 17:1,567–1,582, <http://dx.doi.org/10.1080/01431169608945364>.
- Jackson, C.R., and J.R. Apel, eds. 2004. *Synthetic Aperture Radar Marine User's Manual*. NOAA NESDIS Office of Research and Applications, Washington, DC, 464 pp. Available online at <http://www.sarusersmanual.com> (accessed September 23, 2013).
- Jackson, C.R., J.C.B. da Silva, G. Jeans, W. Alpers, and M.J. Caruso. 2013. Nonlinear internal waves in synthetic aperture radar. *Oceanography* 26(2):68–79, <http://dx.doi.org/10.5670/oceanog.2013.32>.
- Johannessen, J.A., R.A. Shuchman, G. Digranes, D.R. Lyzenga, C. Wackerman, O.M. Johannessen, and P.W. Vachon. 1996. Coastal ocean fronts and eddies imaged with ERS-1 synthetic aperture radar. *Journal of Geophysical Research* 101(C3):6,651–6,667, <http://dx.doi.org/10.1029/95JC02962>.
- Jones, C.E., B. Minchew, B. Holt, and S. Hensley. 2011. Studies of the Deepwater Horizon oil spill with the UAVSAR radar. Pp. 33–50 in *Monitoring and Modeling the Deepwater Horizon Oil Spill: A Record-Breaking Enterprise*. Y. Liu, A. MacFadyen, Z.-G. Ji, and R.H. Weisberg, eds, Geophysical Monograph Series, vol. 195, American Geophysical Union, Washington, DC, <http://dx.doi.org/10.1029/2011GM001113>.
- Karimova, S. 2012. Spiral eddies in the Baltic, Black and Caspian seas as seen by satellite radar data. *Advances in Space Research* 50:1,107–1,124, <http://dx.doi.org/10.1016/j.asr.2011.10.027>.
- Karimova, S.S., and M. Gade. In press. Eddies in the Red Sea as seen by satellite SAR imagery. In *Remote Sensing of the African Seas*. V. Barale and M. Gade, eds, Springer.
- Kim, D.-J., W.M. Moon, and Y.-S. Kim. 2010. Application of TerraSAR-X data for emergent oil-spill monitoring. *IEEE Transactions on Geoscience and Remote Sensing* 48:852–863, <http://dx.doi.org/10.1109/TGRS.2009.2036253>.
- Lavrova, O., M. Mityagina, T. Bocharova, and M. Gade. 2008. Multisensor observation of eddies and mesoscale features in coastal zones. Pp. 463–474 in *Remote Sensing of the European Seas*. V. Barale and M. Gade, eds, Springer, Heidelberg.
- Lehner, S., A. Pleskachevsky, D. Velotto, and S. Jacobsen. 2013. Meteo-marine parameters and their variability observed by high-resolution satellite radar images. *Oceanography* 26(2):80–91, <http://dx.doi.org/10.5670/oceanog.2013.36>.
- Mallas, P.A., and H.C. Graber. 2013. Imaging ships from satellites. *Oceanography* 26(2):150–155, <http://dx.doi.org/10.5670/oceanog.2013.71>.
- Mitnik, L., W. Alpers, K.S. Chen, and A.J. Chen. 2000. Manifestations of internal solitary waves on ERS SAR and SPOT images: Similarities and differences. Pp. 1,857–1,859 in *Proceedings of the 2000 International Geoscience and Remote Sensing Symposium (IGARSS 2000)*, vol. 5, July 24–28, 2000, Honolulu, HI, <http://dx.doi.org/10.1109/IGARSS.2000.858146>.
- Mitnik, L.M., and V.A. Dubina. 2010. Interpretation of SAR signatures of the sea surface: Multisensor approach. Pp. 113–130 in *Oceanography from Space, Revisited*. V. Barale, J.F.R. Gower, and L. Alberotanza, eds, Springer, Dordrecht.
- Mitnik, L.M., V.A. Dubina, and O.G. Konstantinov. 2006. Envisat ASAR polarization experiments in Peter the Great Bay, Japan Sea: Preliminary results. *EARSeL eProceedings* 5(2):199–207. Available online at: <http://www.earsel.org/symposia/2005-symposium-Porto/pdf/094.pdf> (accessed September 23, 2013).
- Mityagina, M., O. Lavrova, and T. Bocharova. 2007. Detection and discrimination of sea surface films in the coastal zone of northeastern Black Sea using SAR data. Abstract ESA SP-636 in *Proceedings of ENVISAT Symposium 2007*, April 23–27, 2007, Montreux, Switzerland.
- Mityagina, M.I., O.Yu. Lavrova, and S.S. Karimova. 2010. Multi-sensor survey of seasonal variability in coastal eddy and internal wave signatures in the northeastern Black Sea. *International Journal of Remote Sensing* 31:4,779–4,790, <http://dx.doi.org/10.1080/01431161.2010.485151>.
- Nunziata, F., P. Sobieski, and M. Migliaccio. 2009. The two-scale BPM scattering model for sea biogenic slicks contrast. *IEEE Transactions on Geoscience and Remote Sensing* 47:1,949–1,956, <http://dx.doi.org/10.1109/TGRS.2009.2013135>.
- Nunziata, F., A. Gambardella, and M. Migliaccio. 2013. On the degree of polarization for SAR sea oil slick observation. *ISPRS Journal of Photogrammetry and Remote Sensing* 78:41–49, <http://dx.doi.org/10.1016/j.isprsjprs.2012.12.007>.
- Porter, D.L., D.R. Thompson, W. Alpers, and R. Romeiser. 2001. Remotely sensed ocean observations of the Coastal Mixing and Optics site from synthetic aperture radars and advanced very high resolution radiometers. *Journal of Geophysical Research* 106(C5):9,623–9,637, <http://dx.doi.org/10.1029/2000JC900121>.
- Wismann, V., M. Gade, W. Alpers, and H. Hühnerfuss. 1998. Radar signatures of marine mineral oil spills measured by an airborne multi-frequency multi-polarization microwave scatterometer. *International Journal of Remote Sensing* 19:3,607–3,623, <http://dx.doi.org/10.1080/014311698213849>.
- Wu, J. 1975. Wind-induced drift currents. *Journal of Fluid Mechanics* 68:49–70, <http://dx.doi.org/10.1017/S0022112075000687>.
- Zatsepin, A.G., A.I. Ginzburg, A.G. Kostianov, V.V. Kremenetskiy, V.G. Krivosheya, S.V. Stanichny, and P.M. Poulain. 2003. Observations of Black Sea mesoscale eddies and associated horizontal mixing. *Journal of Geophysical Research* 108, 3246, <http://dx.doi.org/10.1029/2002JC001390>.